RSC Advances

PAPER

View Article Online
View Journal | View Issue

Cite this: *RSC Adv.*, 2017, **7**, 50610

Synthesis, crystallographic characterization and homogeneous catalytic activity of novel unsymmetric porphyrins†

A. R. Antonangelo,[a] K. C. M. Westrup,[a] L. A. Burt,[b] C. Grazia Bezzu,[b] T. Malewschik,[a] G. S. Machado,[c] F. S. Nunes,[a] N. B. McKeown*[b] and S. Nakagaki*[a]

Received 7th August 2017
Accepted 23rd October 2017

DOI: 10.1039/c7ra08734a

rsc.li/rsc-advances

Unsymmetric porphyrins, containing both pentafluorophenyl (**PFP** = A) and 3,4-dimethoxyphenyl (**DMP** = B) substituents at the *meso* positions, were prepared using Lindsey's methodology. The isomeric *trans*-A_2B_2 (P**1**) and *cis*-A_2B_2 (P**2**) porphyrins together with the tris(pentafluorophenyl)porphyrin A_3B (P**3**) were isolated using chromatography. The porphyrins were characterized by UV-VIS, ^{1}H NMR spectroscopy, mass spectrometry, elemental analysis (C, H, N) and cyclic voltammetry (CV), and their molecular structures were confirmed by single crystal XRD. Their manganese complexes, MnP**1**, MnP**2** and MnP**3**, were also synthesised and used as catalysts in cyclooctene and cyclohexane oxidation reactions under homogeneous conditions. The catalytic studies were supported by electrochemical measurements and showed that the number of electron-withdrawing substituents on the porphyrins rings influences the catalytic activity. These porphyrins may be used as precursors for the design of new materials, such as Polymers of Intrinsic Microporosity (PIMs).

Introduction

Porphyrins are macrocyclic compounds with a large extended conjugated π-system and they are often called "the pigments of life", as they play an important role in many biological systems.[1] These compounds and their metallated complexes exhibit unique properties[2] and can be synthesized through various methodologies.[3] The macrocycles also show great flexibility towards structural modification which makes them very interesting molecules in a number of different fields.[4]

Metalloporphyrins, especially those containing Fe(III) and Mn(III) cations, have been extensively used as catalysts in oxidation reactions of a range of organic compounds using different oxidants. Studies have shown that the introduction of electron-withdrawing and/or bulky substituents at the *ortho* position of the *meso*-phenyl porphyrins (so called second generation porphyrins) can enhance their catalytic activity in oxidation reactions.[5–7] This performance stems from the electronic effects that the substituents exert on the porphyrin ring, which enhances the electrophilicity of the active catalytic species (metal-oxo porphyrin) and also protects the ring, to some extent, against auto oxidative destruction.[6,7] In this context, the free base ligand [5,10,15,20-tetrakis (pentafluorophenyl)porphyrin], [H_2(TPFPP)], represents an important compound.[6–8] The fluorine atoms on the phenyl ring at the four *meso* positions increases the stability and catalytic activity. In addition, the fluorine at *para* positions can be readily substituted by nucleophiles, which makes this compound a versatile platform for the design of new materials.[8,9] Several materials have been recently prepared, which utilize the [H_2(TPFPP)] porphyrin in a heterogeneous catalytic system.[8,10–13] McKeown and co-workers used [H_2(TPFPP)] porphyrin as a monomer in a polymerization reaction with 5,5′,6,6′-tetrahydroxy-3,3,3′,3′-tetramethyl-1,1′-spirobisindane (biscatechol) to prepare a porphyrin network PIM (so called polymer of intrinsic microporosity).[12] The high surface area (up to 1000 $m^2\ g^{-1}$) and the chemical stability of this material encourages the synthesis of new network PIMs and their application in heterogeneous oxidation catalysis.[12–14]

Meso substituted A_2B_2 *trans*-porphyrins bearing different functional groups are useful building blocks for the design and synthesis of new materials with a wide range of applications, such as biomimetic systems and molecular materials.[15–17] The *trans* pattern of substitution in these kinds of porphyrins can be used to achieve new materials with well-defined structures. For example, the same polymerization reaction previously used to synthesize the porphyrin network PIM, could be employed utilizing one *meso–trans* A_2B_2 porphyrin as a preformed monomer in order to achieve new soluble ladder PIMs. Moreover,

[a]*Laboratório de Bioinorgânica e Catálise, Departamento de Química, Universidade Federal do Paraná, Curitiba, 81531-990, Brazil. E-mail: shirleyn@ufpr.br*

[b]*EastChem School of Chemistry, University of Edinburgh, Edinburgh, Scotland, EH9 3FJ, UK. E-mail: neil.mckeown@ed.ac.uk*

[c]*Centro de Estudos do Mar, Pontal do Paraná-PR, Universidade Federal do Paraná (UFPR), Brazil*

† Electronic supplementary information (ESI) available. CCDC 1483009, 1536642 and 1536643. For ESI and crystallographic data in CIF or other electronic format see DOI: 10.1039/c7ra08734a

transition metal ions may also be coordinated to the porphyrin units for future investigation in catalytic membranes.[14] Thus, we undertook the synthesis of a group of new unsymmetric porphyrins with either pentafluorophenyl (**PFP** = A) or 3,4-dimethoxyphenyl (**DMP** = B) at the four *meso* positions.

Experimental

Materials

All chemicals used in this study were purchased from Sigma-Aldrich, Merck or Fluka and were of analytical grade. Iodosylbenzene (PhIO) was synthesized according to the literature.[18] The solid was carefully dried under reduced pressure and kept at 5 °C; its purity was assessed by iodometric titration.[19]

^{1}H and ^{13}C NMR spectra were recorded on Bruker Advance III 500 MHz spectrometers, using deuterated chloroform as solvent. Chemical shifts are reported in ppm (δ) and coupling constants (J) are given in Hz. The multiplicities of the signals in the ^{1}H NMR spectra are abbreviated by s (singlet), d (doublet), q (quartet) and m (multiplet). Mass spectra were acquired on a Bruker Ultraflex MALDI-TOF or Thermo Electron MAT900 mass spectrometers (MALDI or EI). Electronic spectra (UV-VIS) were obtained from dichloromethane solutions on a Hewlett-Packard HP 8452A diode array spectrophotometer in the 200–800 nm range. Analysis were accomplished with a 1 cm path length cell. Fourier Transform Infrared (FTIR) spectra were measured on a Biorad 3500 GX spectrophotometer in the 400–4000 cm^{-1} range with a spectral resolution of 4 cm^{-1}. Elemental analysis were obtained from a Series II 2400 Perkin Elmer Elemental Analyzer. Electron paramagnetic resonance (EPR) measurements of the powdered new manganese porphyrins were conducted on an EPR Bruker EMX MicroX spectrometer (frequency X, band 9.5 GHz) at room temperature and 77 K (liquid N_2), by using perpendicular microwave polarization X-band.

Cyclic voltammetry (CV) was carried out with an IVIUM CompactStat potentiostat/galvanostat. A glassy carbon electrode was employed for the measurements at I = 0.1 mol L^{-1} kept constant with $TBAPF_6$ (tetrabutylammonium hexafluorophosphate). A silver wire and a platinum wire were used as pseudo-reference and auxiliary electrodes, respectively. Ferrocene was used as an internal standard reference and potentials are reported *versus* the standard hydrogen electrode, SHE. Experiments were conducted with a 1.0 × 10^{-3} mol L^{-1} complex concentration in dichloromethane solutions at ambient temperature and under argon atmosphere.

Synthesis and characterization

Preparation of 5-(3,4-dimethoxyphenyl)dipyrromethane. The dipyrromethane was synthesized by Lindsey's methodology[20] using a solution of 3,4-dimethoxybenzaldehyde (1.2 g, 7.22 mmol) and freshly distilled pyrrole (20 mL, 288 mmol) followed by the addition of trifluoroacetic acid (TFA) (55 μL, 0.72 mmol). The product was purified by chromatography column (6 cm diameter × 20 cm height, silica, pore size: 60 Å, 40–63 μm) using a mixture of solvents: petroleum ether : ethylacetate : triethylamine (80 : 20 : 1). The solid (pale yellow) was then triturated with hexane and filtered, yielding a colourless solid (1.29 g, 63.2% yield). Molecular formula: $C_{17}H_{18}N_2O_2$. ^{1}H NMR data (500 MHz, $CDCl_3$, 298 K) δ ppm: 7.95 (s, 2H, N*H* pyrrole), 6.85–6.84 (d, 1H, J = 8.1 Hz, Ar*H*), 6.79–6.76 (m, 2H, Ar*H*), 6.73–6.72 (m, 2H, C*H* pyrrole), 6.20–6.18 (q, 2H, J = 2.8 Hz, C*H* pyrrole), 5.98–5.96 (m, 2H, C*H* pyrrole); 5.46 (s, 1H, C*H* *meso*), 3.90 (s, 3H, –OCH_3), 3.83 (s, 3H, –OCH_3). ^{13}C NMR data (125 MHz, $CDCl_3$, 298 K) δ ppm: 149.1, 148.1, 134.6, 132.7, 120.3, 117.1, 111.8, 111.2, 108.5, 107.1, 56.0, 55.9, 43.6. LRMS (EI): m/z 282.1 (M^+), according to the literature data.[21]

Preparation of free base porphyrins P1, P2 and P3, and their manganese complexes MnP1, MnP2 and MnP3. The free base porphyrins were synthesized by Lindsey methodology[22] using 5-(3,4-dimethoxyphenyl)dipyrromethane (1.29 g; 4.57 mmol) and pentafluorobenzaldehyde (0.9 g, 4.57 mmol) dissolved in dry CH_2Cl_2 (460 mL) followed by the addition of TFA (0.6 mL; 8.13 mmol). The solution was stirred under N_2 atmosphere at room temperature for 50 min. Then, 2,3-dichloro-5,6-dicyano-1,4-benzoquinone (1.34 g, 5.90 mmol) was added and the resultant solution was stirred further for 1 h. The resulting crude product was purified over two successive chromatography columns (silica, 6 cm diameter × 30 cm height, CH_2Cl_2), where it was possible to isolate the three porphyrins: **P1** (R_f = 0.75), **P2** (R_f = 0.61) and **P3** (R_f = 0.84).

Porphyrin P1. Purple solid (0.134 g, 6.4% yield). Elemental analysis (%) calcd. for $C_{48}H_{28}F_{10}N_4O_4$: C 63.03, H 3.09, N 6.12. Found: C 62.97, H 3.18, N 5.73.^{1}H NMR data (500 MHz, $CDCl_3$, 298 K) δ ppm = 9.04–9.03 (d, 4H, J = 4.8 Hz, *H*β-pyrrolic), 8.82–8.81 (d, 4H, J = 4.8 Hz, *H*β-pyrrolic), 7.80–7.78 (m, 4H, Ar*H*), 7.32–7.30 (d, 2H, J = 7.9 Hz, Ar*H*); 4.22 (s, 6H, –OCH_3), 4.03 (s, 6H, –OCH_3), −2.78 (s, 2H, N*H*). UV-VIS in CH_2Cl_2 at 298 K, λ_{max} (log ε/M − 1 cm^{-1}): 420 (5.38), 512 (4.25), 548 (3.77), 588 (3.76) and 644 (3.51). FT-IR data (cm^{-1}, KBr pellet): 3321, 3116, 2933, 1517, 1496, 1479, 1465, 1440, 1406, 1353, 1346, 1319, 1257, 1237, 1166, 1139, 1076, 1041, 1027, 987, 923, 919, 813, 802, 779, 756, 734. MALDI-TOF-MS (m/z): 914.1 $[MH]^+$.

Porphyrin P2. Purple solid (0.055 g, 2.6% yield). Elemental analysis (%) calcd. for $C_{48}H_{28}F_{10}N_4O_4$: C 63.03, H 3.09, N 6.12, found: C 63.13, H 3.18, N 5.72.^{1}H NMR data (500 MHz, $CDCl_3$, 298 K) δ ppm: 9.04–9.03 (d, 2H, J = 4.8 Hz, *H*β-pyrrolic), 8.95 (s, 2H, *H*β-pyrrolic), 8.87 (s, 2H, *H*β-pyrrolic), 8.79–8.78 (d, 2H, J = 4.8 Hz, *H*β-pyrrolic), 7.80–7.76 (m, 4H, Ar*H*), 7.31–7.29 (d, 2H, J = 8.1 Hz, Ar*H*), 4.21 (s, 6H, –OCH_3); 4.03 (s, 6H, –OCH_3), −2.70 (s, 2H, N*H*). UV-VIS in CH_2Cl_2 at 298 K, λ_{max} (log ε/M − 1 cm^{-1}): 421 (5.39), 514 (4.24), 550 (3.74), 588 (3.78) and 642 (3.22). FT-IR data (cm^{-1}, KBr pellet): 3321, 3105, 2931, 1515, 1498, 1479, 1463, 1440, 1404, 1350, 1321, 1257, 1238, 1166, 1139, 1120, 1081, 1041, 1027, 987, 918, 865, 802, 761, 742. MALDI-TOF-MS (m/z): 914.1 $[MH]^+$.

Porphyrin P3. Purple solid (0.01 g, 0.5% yield). Elemental analysis (%) calcd. for $C_{46}H_{19}F_{15}N_4O_2$: C 58.49, H 2.03, N 5.93, found: C 57.06, H 1.84, N 5.68.^{1}H NMR data (500 MHz, $CDCl_3$, 298 K) δ ppm: 9.06–9.05 (d, 2H, J = 4.8 Hz, *H*β-pyrrolic), 8.90 (m, 4H, *H*β-pyrrolic), 8.83–8.82 (d, 2H, J = 4.8 Hz, *H*β-pyrrolic), 7.79–7.77 (m, 2H, Ar*H*); 7.32–7.30 (d, 1H, J = 8.0, Ar*H*), 4.22 (s, 3H, –OCH_3), 4.03 (s, 3H, –OCH_3), −2.79 (s, 2H, N*H*). UV-VIS in

CH_2Cl_2 at 298 K, λ_{max} (log ε/M − 1 cm^{-1}):415 (5.41), 510 (4.31), 544 (3.71), 586 (3.90) and 638 (3.30). FT-IR data (cm^{-1}, KBr pellet): 3321, 3107, 2933, 1517, 1498, 1483, 1467, 1438, 1402, 1352, 1342, 1319, 1257, 1240, 1166, 1143, 1078, 1058, 1045, 1027, 989, 925, 918, 802, 756, 736. MALDI-TOF-MS (*m*/*z*): 944.1 $[MH]^+$.

The free base porphyrins P**1**, P**2** and P**3** were metallated by a methodology described in the literature[23] using manganese(II) acetate as metal salt. The process was monitored by TLC and UV-VIS techniques. The complexes were purified by column (CH_2Cl_2 and MeOH) and the excess of salt was removed by washing the metalloporphyrins solids with plenty of warm water. The new metalloporphyrins, designated Mn**P1**, Mn**P2** and Mn**P3**, respectively, were characterized by UV-VIS spectroscopy (ESI: Fig. S7†) and EPR technique was used to confirm the oxidation state of manganese and also to confirm the absence of manganese(II) acetate (ESI: Fig. S8†).

Single crystal X-ray diffraction

Single crystal X-ray diffraction data were collected on either a i19-FFD-air (fixed Chi) Pilatus M2 at the Diamond Light source Beam line I19-1 (P**1**) or a Rigaku Oxford Diffraction Super Nova (P**2** and P**3**) diffractometer using synchrotron (0.6889 Å) or Cu-K_α (1.5418 Å) radiation, respectively. The crystal temperature was controlled using an Oxford Cryo systems Cryo stream 700+ low temperature device for all of the samples. All data were processed using Crysalis Pro. Crystal structure solutions were achieved using intrinsic phasing with ShelXT and refined using least squares minimization with the ShelXL refinement package interfaced with Olex2.[24,25] In structures P**2** and P**3** N-bound hydrogens were identified from a difference Fourier map and refined with appropriate geometric restraints. C-bound H atoms in all structures were placed in calculated geometric positions and refined using the riding model. Crystallographic data for structures P**1**, P**2** and P**3** have been deposited at the Cambridge Crystallographic Data Center. CCDC: 1483009, 1536642 and 1536643. Further crystallographic data can be found in the ESI.†

Catalytic studies of MnP1, MnP2 and MnP3 using (*Z*)-cyclooctene and cyclohexane as substrates

The catalytic activity and efficiency of the new metalloporphyrins was tested in the oxidation reactions of (*Z*)-cyclooctene (previously purified on alumina column) and cyclohexane with iodosylbenzene (PhIO). Furthermore, the two associated symmetric metalloporphyrins, (5,10,15,20-tetrakis-pentafluorophenyl)porphyrin manganese(III), Mn**TPFPP**, and 5,10,15,20-tetrakis-(3,4-dimethoxyphenyl)porphyrin manganese(III), Mn**TDMPP**, were also used as catalysts for comparison.

The catalytic reactions were performed in a 1.5 mL glass flask equipped with a magnetic stirrer, in a dark chamber. The solvent mixture (acetonitrile/dichloromethane, ACN : DCM 1 : 1, v/v) and the substrates were purged with argon for 15 min. The catalysts (Mn**P1**, Mn**P2**, Mn**P3**, Mn**TPFPP** and Mn**TDMPP**) and the oxidant PhIO (catalyst/PhIO at a molar ratio of 1 : 10) were added in the reaction flask and they were also purged with argon for 15 min. Then, the mixture of solvents (ACN : DCM, 1 : 1) was added to the reactions flasks, followed by addition of the substrates (*Z*)-cyclooctene or cyclohexane. The molar ratio (catalyst/PhIO/substrate) used was 1 : 10 : 1000 which was calculated based on the molecular mass of the metalloporphyrins (about 0.5 mg of metalloporphyrins were used for each reaction). The oxidation reactions were performed under magnetic stirring for 1 h, at room temperature, in the absence of light. After 1 h, the excess of iodosylbenzene was consumed by addition of sodium sulfite and the reaction mixture was transferred to a volumetric flask (2 mL). The resulting solution containing the reaction products was analyzed by gas chromatography using bromobenzene or 1-pentanol as internal standards. The products from the oxidation reactions were quantified with an Agilent 6850 gas chromatograph (flame ionization detector) equipped with a 30 m long DB-WAX capillary column with 0.25 mm internal diameter (J&W Scientific). Product yields were based on the quantity of PhIO added to each reaction.

Results and discussion

Porphyrin synthesis

It was anticipated that the porphyrin *meso trans*-A_2B_2(P**1**) would be synthesized using Lindsey's methodology,[20,22] between 5-(3,4-dimethoxyphenyl)dipyrromethane and pentafluorobenzaldehyde (Scheme 1). Analysis of the crude product mixture revealed that the desired porphyrin P**1** was prepared along with the *cis*-A_2B_2 isomer P**2** and the tris-pentafluorophenylporphyrin A_3B (P**3**) (Scheme 1). The formation of P**2** and P**3** is probably associated with scrambling of the phenyl substituents due to acidolysis and recombination of dipyrromethanes.[26,27] The yield for the desired porphyrin (P**1**) was low (6.4%), but respectable in comparison with that of the isomeric unsymmetric porphyrin 5,15-bis(3,5-dimethoxyphenyl)-10,20-bis(pentafluorophenyl) (3.8%), prepared using the mixed aldehyde methodology.[28]

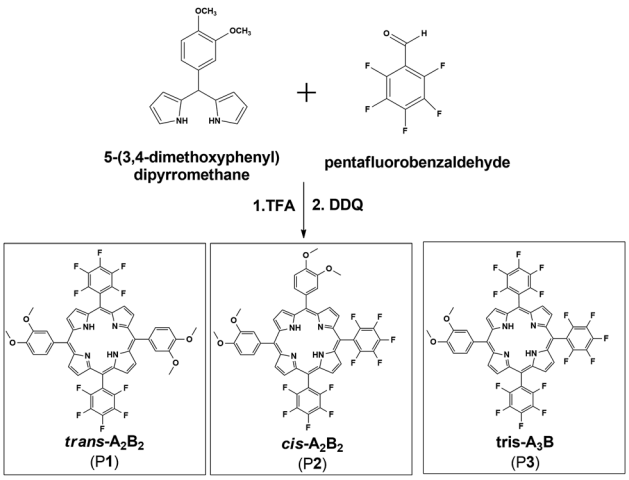

Scheme 1 Schematic representation of the free-base porphyrins preparation.

The ^{1}H NMR spectroscopy was fundamental for differentiation between the *trans*-A_2B_2 (**P1**) and *cis*-A_2B_2 (**P2**) isomers (Table 1 and ESI: Fig. S3–S5†). The D_{2h} symmetry of *trans*-A_2B_2 molecule (**P1**) gives specific signal patterns with two doublets for the β-pyrrole protons at 9.0 and 8.8 ppm, while the lower symmetry in the *cis*-A_2B_2 (**P2**) compared to the *trans* **P1** isomer[29] gives rise to two singlets at 8.9 and 8.8 ppm and two doublets at 9.0 and 8.7 ppm. In the tris-A_3B molecule (**P3**) the β-pyrrole protons are split up into two doublets at 9.0 and 8.8 ppm and one multiplet at 8.9 ppm. These results are in agreement with the basic patterns of splitting of the β-pyrrole protons in unsymmetric porphyrins as reported for Meng and co-workers.[29]

The UV-VIS spectra of the porphyrin macrocycle are consistent with the D_{2h} micro-symmetry according to the Four-Orbital Model developed by Gouterman (ESI: Fig. 6†).[30] The spectra of the free base porphyrins shows an intense absorption near 400 nm (Soret band) and four less intense bands (Q bands) labeled as IV, III, II and I, between 450 and 700 nm. In general, electron-donating substituents lead to red shifts for both the Soret and Q bands.[30–35] The electronic coupling between electron-donating groups and the porphyrin core in **P1**–**P3** decreases the HOMO–LUMO energy gaps and causes a red shift in its spectra compared to the free base porphyrin H_2T**PFP**P (ESI: Fig. 6†).

Furthermore, it is well established that the relative intensity of the four Q bands is dependent on the substituent groups at the macrocycle periphery. According to the relative intensities, the four visible Q bands are classified as etio, rhodo, oxorhodo, and phyllo.[30,36] The porphyrins **P1**–**P3** give a phyllo spectra (with intensities IV > II > III > I), which is in agreement with *meso*-phenyl porphyrins spectra. The reduction in the intensities of bands III and I observed in the spectrum of the porphyrin **P3** may be attributed to the restricted rotation of the phenyl groups resulting from steric interaction of the *ortho*-fluorine substituent and the β-pyrrole hydrogens.[36]

The metalation process of the free base porphyrins **P1**, **P2** and **P3** with manganese(II) acetate was monitored by recording the electronic spectra at different reaction times. The bathochromic shift observed in the Soret band is characteristic of Mn(III) porphyrins, which confirms the formation of Mn**P1**, Mn**P2** and Mn**P3**[37] (ESI: Fig. S7†). These new metalloporphyrins were also characterized by solid state EPR (ESI: Fig. S8†) and no signal was observed at room temperature or 77 K, in agreement with presence of Mn(III) in the porphyrin core.[5,38] Indeed, the Mn(III) ions has four unpaired d electrons with $S = 2$, typically featuring a pronounced Jahn–Teller distortion which results in substantial spin–orbit coupling.[38] Thereby, the coupling and rapid spin relaxation process results in absence of signal in mononuclear Mn(III) EPR spectra even at 77 K (under perpendicular microwave polarization).[5,38]

Furthermore, the EPR confirms that the excess of manganese(II) acetate, which shows a signal in $g = 2$ (ESI: Fig. S8†), was removed during the purification of the new metalloporphyrins (through column and washing with warm water).

Single crystal X-ray diffraction

Each one of the free base porphyrins **P1**, **P2** and **P3** was successfully characterized by single crystal XRD that allowed unambiguous confirmation of each structure. Suitable crystals were grown *via* slow vapour diffusion of methanol into chloroform solution. Crystal data, data collection and structure refinement can be found in the ESI.† Selected crystallographic and geometric parameters for each structure are also shown in Table 2. Crystals of **P1**, **P2** and **P3** form monoclinic unit cells belonging to the space groups $P2_1/c$, $I2/a$ and Cc, respectively. The ORTEP[39] and molecular crystal packing diagrams for each porphyrin are shown in Fig. 1.

The unsymmetric units of **P1** and **P2** contain one-half of each molecule, along with one molecule of chloroform. The porphyrin rings are both relatively flat, with the largest deviation from planarity being 0.04 Å and 0.09 Å for **P1** and **P2** respectively, demonstrating little difference for the *cis* or *trans*-isomer. The dihedral angle between the **DMP** substituents and the porphyrin ring appear to be relatively similar for both **P1** and **P2**, varying from 66.4 to 67.9°, with the **PFP** groups of **P1** also within this range. However, the **PFP** groups of **P2** adopt a close to perpendicular orientation to the macrocycle, with an angle of 86.0°.

The porphyrin macrocycles in the crystal structures of **P1** and **P2** are arranged in a herring bone and off-set stacked crystal packing motif, respectively (Fig. 1b and d). Analysis of the packing in the crystal of **P1** reveals a variety of close intermolecular interactions between each of the macrocycles, of which C···H, C···O, H···N, F···H, F···C and F···F interactions are present. Despite the similarities in the chemical composition of **P1** and **P2**, fewer types of interactions could be observed in the crystal structure of **P2**, attributed to the relative positions of the substituted phenyl substituents. The crystal structure of **P2** contains C···F, F···H, F···C and O···H close interactions, with

Table 1 ^{1}H Chemical shift data (δ, ppm) for *trans*-A_2B_2 (**P1**), *cis*-A_2B_2 (**P2**) and tris-A_3B (**P3**) in $CDCl_3$. Multiplicity and integration in parentheses

	H-β-pyrrolic	Ar*H*	–O*CH*$_3$	N*H*
Trans-A_2B_2 (**P1**)	9.04–9.03 (d, 4H) 8.82–8.81 (d, 4H)	7.80–7.78 (m, 4H) 7.32–7.30 (d, 2H)	4.22 (s, 6H) 4.03 (s, 6H)	−2,78 (s, 2H)
Cis-A_2B_2 (**P2**)	9.04–9.03 (d, 2H) 8.95 (s, 2H) 8.87 (s, 2H) 8.79–8.78 (d, 2H)	7.80–7.76 (m, 4H) 7.31–7.29 (d, 2H)	4.21 (s, 6H) 4.03 (s, 6H)	−2,70 (s, 2H)
Tris-A_3B (**P3**)	9.06–9.05 (d, 2H) 8.9 (m, 4H) 8.83–8.82 (d, 2H)	7.79–7.77 (m, 2H) 7.32–7.30 (d, 1H)	4.22 (s, 3H) 4.03 (s, 3H)	−2,79 (s, 2H)

Table 2 Selected crystallographic and geometric parameters for the crystal structure of P1, P2 and P3

	P1	P2	P3
Empirical formula	$C_{50}H_{30}Cl_6F_{10}N_4O_4$	$C_{50}H_{30}Cl_6F_{10}N_4O_4$	$C_{47}H_{22}F_{15}N_4O_3$
Formula weight	1153.48	1153.48	975.68
Temperature/K	100	200	120
Crystal system	Monoclinic	Monoclinic	Monoclinic
Space group	$P2_1/c$	$I2/a$	Cc
a/Å	13.948(3)	12.0821(2)	11.5360(2)
b/Å	15.6771(17)	17.9808(2)	26.8989(6)
c/Å	11.2006(16)	22.7546(3)	15.0809(3)
β/°	109.177(18)	96.0320(10)	109.961(2)
Volume/Å^3	2313.2(7)	4915.97(12)	4398.56(16)
Z	2	4	4
2Θ range for data collection/°	2.996 to 40.268	6.278 to 152.246	6.240 to 152.16
Reflections collected	8341	39 378	35 755
Independent reflections	2340 [$R_{int} = 0.0857$, $R_{sigma} = 0.0726$]	5127 [$R_{int} = 0.0661$, $R_{sigma} = 0.0289$]	7617 [$R_{int} = 0.0660$, $R_{sigma} = 0.0400$]
Final R indexes [$I \geq 2\sigma(I)$]	$R_1 = 0.0725$, w$R_2 = 0.1897$	$R_1 = 0.0659$, w$R_2 = 0.1874$	$R_1 = 0.1043$, w$R_2 = 0.2897$
Final R indexes [all data]	$R_1 = 0.1160$, w$R_2 = 0.2565$	$R_1 = 0.0708$, w$R_2 = 0.1943$	$R_1 = 0.1079$, w$R_2 = 0.3001$
CCDC deposition number	1483009	1536642	1536643

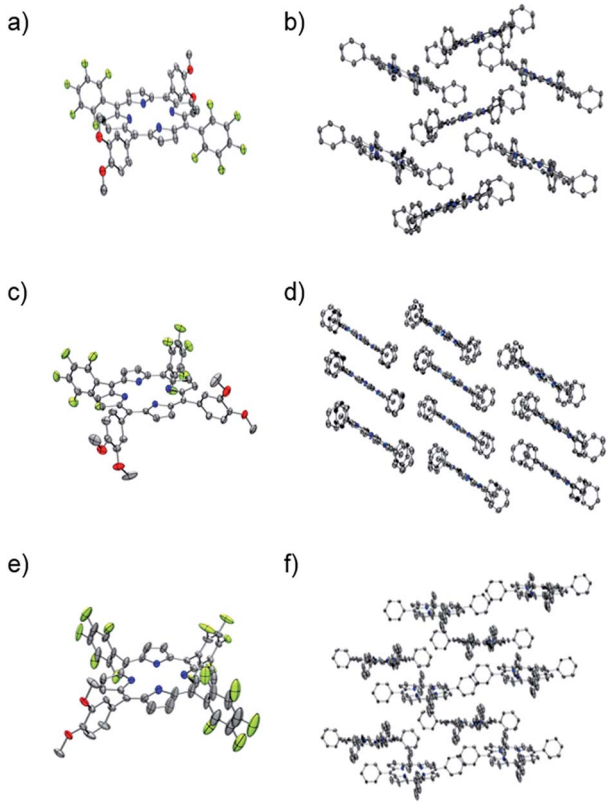

Fig. 1 ORTEP molecular diagrams of (a) P1, (c) P2 and (e) P3 where the solvent molecules and hydrogens have been omitted for clarity. Thermal ellipsoids are also shown at 50% probability for P1 and P2 and 35% probability for P3. Crystal packing diagrams for (b) P1, (d) P2 and (f) P3 where the solvent molecules and hydrogen, oxygen and fluorine atoms have been omitted for clarity. Thermal ellipsoids are also shown at 50% probability for P1 and P2 and 35% probability for P3.

the O···H close contacts generated by the association between the methoxy substituents of each porphyrin (Fig. S12-ESI†).

The unsymmetric unit of P3 contains a complete porphyrin macrocycle with one molecule of methanol. The ring demonstrates a much larger deviation of planarity compared to P1 and P2, with a maximum deviation from planarity of 0.351 Å. The two **PFP** substituents both exhibit significant disorder that could be modelled over two positions but still demonstrate a large amount of libration as shown on the thermal ellipsoids. The disorder appears to coincide with the presence of small voids around the **PFP** substituents, that when combined account for 5.7% (251 Å^3) of the unit cell, as calculated by PLATON VOID.[40]

Further analysis with PLATON SQUEEZE[40] calculated a residual electron count of 47 e$^-$ that corresponds to another possible 0.6 molecules of methanol per molecule of P3. However, their scattering contribution to the overall structure refinement was not removed. The dihedral angle between the substituted phenyl groups varies from 68.4° to 86.3°, with the maximum dihedral angles observed for the two disordered **PFP** rings. The macrocycles within the crystal structure of P3 are arranged in a slip-stacked formation (Fig. 1f), which is arranged *via* a number of O···H, C···H, F···H, F···N, F···C and N···H close interactions and, as expected, a large number of the intermolecular interactions observed involve fluorine.

Cyclic voltammetry of H_2P

Fig. 2 shows the cyclic voltammograms (CV) of the free base porphyrins in CH_2Cl_2 solutions. H_2Ps showed two quasi-reversible oxidations and two quasi-reversible reductions. The oxidations exhibited $E_{1/2}$ potentials that are referred to the SHE as follows: +1.671 V and +1.836 V for P1, +1.632 V and +1.866 V for P2 and +1.829 V and +2.023 V for P3. Reductions were observed at $E_{1/2}$: −0.942 V and −0.536 V for P1, −0.972 V and −0.608 V for P2 and −0.853 V and −0.447 V for P3.

These values clearly show a similar redox behavior for P1 and P2, which is expected since they have the same substituents, and differ only on their geometric configuration, *cis* or *trans*, thus offering the same overall outcome to the electronic density of the porphyrin. In contrast, the unsymmetric porphyrin P3 exhibited a significant resistance to oxidation, in agreement

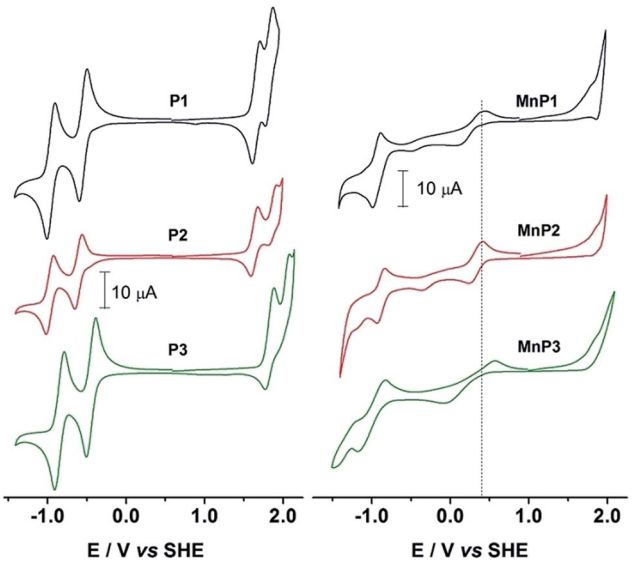

Fig. 2 Cyclic voltammograms of H_2P and MnP in dichloromethane containing 0.1 mol L^{-1} $TBAPF_6$. Scan rate at 100 mV s^{-1}. Initial anodic scan.

with the presence of a higher number of fluoro-atoms, which causes a strong inductive electron withdrawing effect. The mean potential difference between the two oxidations and between the two reductions for H_2Ps are 0.198 V and 0.392 V, respectively. This result is in accordance with analogue cases in the literature for successive monoelectronic ring-centered processes, explained by the formation of porphyrin π-cation/anion radicals and dications/dianions as depicted in Scheme 2.[41,42] Furthermore, the potential difference between the first oxidation and the first reduction, $\Delta E_{1/2(\text{oxi–red})}$, is a good estimate of the band gap between the frontier orbitals HOMO and LUMO. It was found the following order of decreasing $\Delta E_{1/2(\text{oxi–red})}$: **P3** (2.276 V) > **P2** (2.240 V) > **P1** (2.207 V), in accordance with the higher resistance of **P3** towards oxidation. The values for **P3** are slightly higher than the 2.23 V observed for the *meso*-tetraphenylporphyrin [H_2(TPP)],[43] and lower than 2.34 V for 5,10,15,20-tetrakis(pentafluorophenyl)porphyrin [H_2(TPFPP)]. All electrochemical data are collected in Table 3.

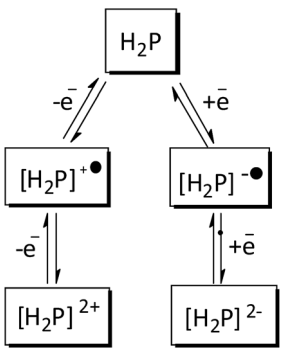

Scheme 2 Schematic representation of monoelectronic process in the formation of porphyrin π-cation/anion radicals and dications/dianions.

Cyclic voltammetry of MnP

The cyclic voltammograms (CV) of manganese(III) porphyrins showed irreversible oxidations starting at +1.8 V, which were assigned to the electrogenerated cation radicals and the dications of the macrocycle ring (Fig. 2). An irreversible reduction of MnP, probably related to the irreversible oxidations, was seen in the range of −0.35 V to −0.48 V along with quasi-reversible reduction processes between −0.926 V and −0.999 V to produce the monoanion radical and dianions porphyrins, in that order. Anodic peak potentials of the quasi-reversible electron transfer centered in the manganese ion were observed at +0.440 V, +0.413 V and +0.558 V, for MnP**1**, MnP**2** and MnP**3**, respectively. The overall electron transfer sequence can be summarized in the following steps: $[Mn^{II}P]^{2-} \rightarrow [Mn^{II}P^{\bullet}]^{-} \rightarrow [Mn^{II}P] \rightarrow [Mn^{III}P]^{+} \rightarrow [Mn^{III}P^{\bullet}]^{+} \rightarrow [Mn^{III}P]^{2+}$.[44,45]

Ucoski and co-workers[46] reported the electrochemistry of the 5,10,15,20-tetrakis(1,3-benzodioxole)-Mn^{III} porphyrin in dichloromethane and observed a $E_{1/2} = -0.61$ V *vs.* SHE for the Mn^{III}/Mn^{II} couple. This result agrees with the donor character of the dioxole substituent, compared to the substituents reported in this work, making the oxidation of the manganese center an easier process in that case. Also for comparison, $E_{1/2}$ of Mn^{III}/Mn^{II}(TPFPP) and of Mn^{IV}/Mn^{III}(TPFPP) were observed in acetonitrile at +0.05 and at +1.75 V *vs.* SHE, repectively.[47]

Catalytic studies of MnP1, MnP2 and MnP3 using (*Z*)-cyclooctene and cyclohexane as substrates

The efficiency of the porphyrins MnP**1**, MnP**2** and MnP**3** and the model compounds MnT**PFP**P and MnT**DMP**P as catalysts in homogeneous oxidation reactions was tested using the substrates (*Z*)-cyclooctene and cyclohexane and iodosylbenzene (PhIO) as an oxidant (Fig. 3). It has been previously shown that electron-withdrawing substituents at the *ortho* position of the *meso*-phenyl substituents in the porphyrin ring can enhance the catalytic activity of these compounds for oxidation reactions.[6,7] Hence, MnT**PFP**P was used as a model catalyst because it is recognized as a highly efficient catalyst in homogeneous oxidation reactions for various substrates.[48,49] Its enhanced performance can be attributed mainly to its greater stability under oxidative conditions, resulting from the electron-withdrawing nature of the **PFP** substituent, which protects, to some extent, the self-destruction of the porphyrin ring. On the other hand, MnT**DMP**P was used as an opposing model catalyst for comparison because it contains only the highly electron-donating **DMP** substituents.

The molecule (*Z*)-cyclooctene is a useful diagnostic substrate as it is easily oxidized in the presence of metalloporphyrins, with (*Z*)-cyclooctene oxide usually being the sole product of reaction.[48–50]

The catalytic activity of the new manganese(III) porphyrins MnP**1**, MnP**2** and MnP**3** using (*Z*)-cyclooctene as a substrate resulted in similar product yields. The new unsymmetric manganese(III) porphyrins also showed analogous catalytic activity to that observed for the completely symmetric porphyrin MnT**PFP**P (~86%) (Fig. 4). This result suggests that the presence of two (MnP**1** and MnP**2**) or one (MnP**3**) 3,4-dimethoxy groups

Table 3 Half-wave potentials (V *vs.* SHE) measured at 100 mV s^{-1} of free base porphyrins and metaloporphyrins in CH_2Cl_2, 0.1 M $TBAPF_6$

	E_{ox1}	E_{ox2}	ΔE_{ox}	E_{red1}	E_{red2}	ΔE_{red}	$(E_{ox1} - E_{red1})^d$	E^a (Mn^{III}/Mn^{II})	Ref.
H_2**TPP**	+0.93	+1.26	0.33	−1.29	−1.62	0.33	2.22	—	41
H_2**TPFPP**	+1.838[a]	+2.123[a]	0.285	−0.543	−0.952	0.409	2.340[c]	—	tw
H_2**TDMPP**	+1.299	+1.433	0.134	−0.965	−1.267	0.302	2.264		tw
P1	+1.671	+1.836	0.165	−0.536	−0.942	0.406	2.207	—	tw
P2	+1.632	+1.866	0.234	−0.608	−0.972	0.364	2.240	—	tw
P3	+1.829	+2.023	0.194	−0.447	−0.853	0.406	2.276	—	tw
Mn**P1**	+1.8[a]	n.o.	—	−0.48[b]	−0.926	0.45	2.3	+0.440[a]	tw
Mn**P2**	+1.8[a]	n.o.	—	−0.35[b]	−0.882	0.53	2.2	+0413[a]	tw
Mn**P3**	+1.8[a]	n.o.	—	n.o.	−0.999	—	—	+0.558[a]	tw

[a] E_{pa}. [b] E_{pc}. [c] $(E_{pa1} - E_{pc1})$. [d] HOMO–LUMO gap; n.o. = not observed; tw = this work.

in the structure of the new synthesized metalloporphyrins does not seem to interfere in their catalytic activity for the oxidation of (*Z*)-cyclooctene. However, the catalytic activity of the completely symmetric Mn**TDMPP** was lower (~73%), which can be attributed to the absence of electron-withdrawing substituent in this porphyrin.[50]

Cyclohexane is a less reactive substrate than (*Z*)-cyclooctene in oxidation reactions and when metalloporphyrins are used as catalysts, both cyclohexanol and cyclohexanone are obtained as major products.[10,48–50] The novel metalloporphyrins reported here have shown alcohol selectivity in the cyclohexane oxidation (Fig. 5), which is in agreement with reported results of homogeneous catalysis using other metalloporphyrins.[48–50]

For the cyclohexane reactions it was possible to observe a trend in the catalytic activity of the fluorine-substituted metalloporphyrins which increased with an increasing number of pentafluorophenyl substituents present in the porphyrin: Mn**P1** ~ Mn**P2** (~40% yield for alcohol) < Mn**P3** (~49%) < Mn**TPFPP** (~54%). The low catalytic activity of the Mn**TDMPP** (~14%) under the reaction conditions is associated with the absence of bulky or electron-withdrawing substituents at the *ortho* position of the *meso*-phenyl macrocycle, which is in agreement with results obtained previously using a similar porphyrin structure.[50]

The oxidation peak potentials (E_{pa}) values of Mn**P1** (+0.440 V), Mn**P2** (+0.413 V) and Mn**P3** (0.558 V) (Table 3) correlates well with their increasing catalytic activity, in that order, towards the oxidation of cyclohexane (Fig. 5). The similarity of E_{pa} for Mn**P1** and Mn**P2** agrees with the close yields (~40%) observed for the cyclohexanol production, while Mn**P3** showed a 49% yield for the alcohol. The higher reduction potential of Mn**P3** compared to the other metalloporphyrins herein reported means that the active intermediate containing the high valent manganese[51–53] IV or V Mn=(O)**P3** is a better oxidant agent due to the increased number of pentafluorophenyl groups in the porphyrin composition, thus, in the course of the reaction, it favors the oxygen transfer to the substrate. Furthermore, the pentafluorophenyl substituents protect the porphyrin from oxidative damage, increasing the turnover numbers and helps increase the yields of the oxidation reactions.

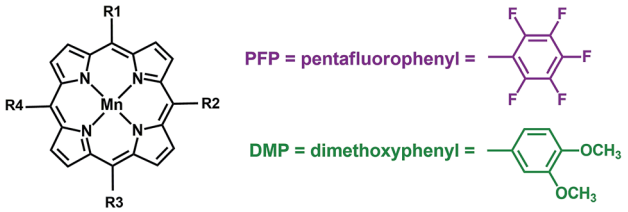

Metalloporphyrins	R1	R2	R3	R4
Mn**P1** (*trans*-A_2B_2)	PFP	DMP	PFP	DMP
Mn**P2** (*cis*-A_2B_2)	DMP	PFP	PFP	DMP
Mn**P3** (tris-A_3B)	PFP	PFP	PFP	DMP
Mn**TPFPP**	PFP	PFP	PFP	PFP
Mn**TDMPP**	DMP	DMP	DMP	DMP

Fig. 3 Structures of porphyrins Mn**P1**, Mn**P2** and Mn**P3**, and the model compounds Mn**TPFPP**, Mn**TDMPP** used as catalysts for (*Z*)-cyclooctene and cyclohexane oxidation reactions.

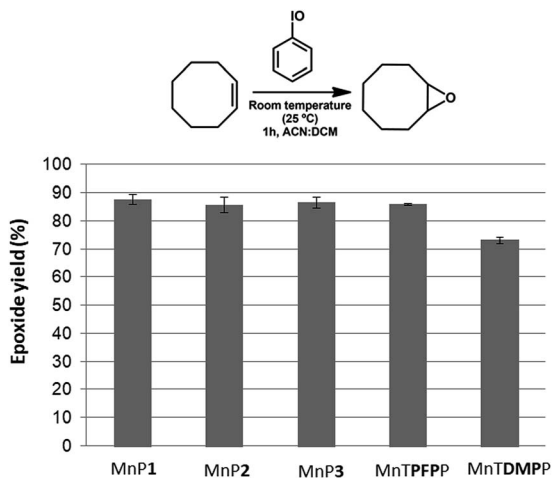

Fig. 4 (*Z*)-Cyclooctene oxidation reaction using PhIO catalyzed by Mn**P1**, Mn**P2**, Mn**P3**, Mn**TPFPP** and Mn**TDMPP**. Catalyst/PhIO/Substrate molar ratio = 1 : 10 : 1000. The product yields were calculated based on the amount of PhIO used in the reactions. Results represent reactions performed in duplicate.

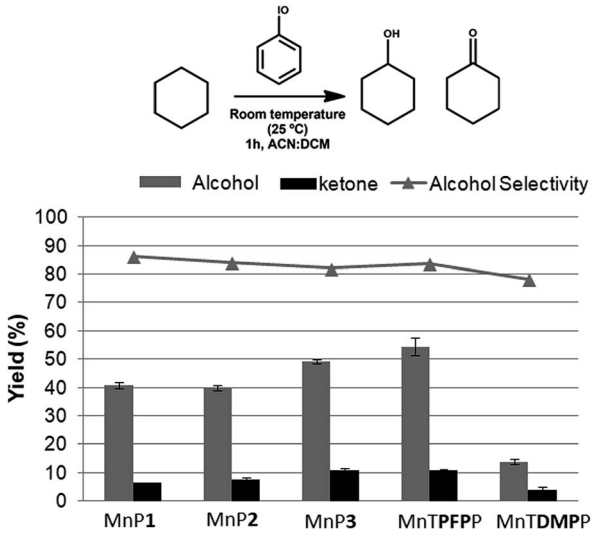

Fig. 5 Cyclohexane oxidation reaction using PhIO catalysed by MnP**1**, MnP**2**, MnP**3**, MnT**PFP**P and MnT**DMP**P. Catalyst/PhIO/Substrate molar ratio = 1 : 10 : 1000. The product yields for cyclohexanol (alcohol) and cyclohexanone (ketone) were calculated based on the amount of PhIO used in the reactions. Results represent reactions performed in duplicate.

Conclusions

In this work the synthesis, characterization and crystal structure of three unsymmetrical free base porphyrins (P**1**, P**2** and P**3**) are reported. The catalytic activity of the metallated unsymmetric porphyrins MnP**1**, MnP**2** and MnP**3**, together with the electrochemical studies, showed that the number of pentafluorophenyl groups on the metalloporphyrin structure (two or three) has a direct influence on their catalytic activity in homogeneous medium. The compound MnP**3**, which has three pentafluorophenyl in its structure, showed better catalytic results, similar to the MnT**PFP**P, and also higher reduction potential compared to the other metalloporphyrins herein reported. These porphyrins are interesting precursors for the design of well-defined new materials, with a focus towards the construction of PIMs that combine high surface area with recognized catalytic properties of metallated porphyrins.

Conflicts of interest

There are no conflicts to declare.

Acknowledgements

The authors are grateful to Coordenação de Aperfeiçoamento de Pessoal de Nível Superior (CAPES), Conselho Nacional de Desenvolvimento Científico e Tecnológico (CNPq) – Science without Borders, Fundação Araucária and Universidade Federal do Paraná (UFPR) for financial support and the authors thank the EPSRC (grant EP/N01331X/1) for funding. Kátia C. M. Westrup thanks Fundação Araucária and Capes for the pos-doctoral scholarship (Convênio 396/2014 – Projeto 41060 – SIT 21045). The authors are also grateful to The University of Edinburgh and acknowledge beam line I19 of the Diamond Light Source (DLS), UK, for assistance in obtaining crystallographic data.

References

1 L. R. Milgrom, *The Colours of Life. An introduction to the Chemistry of Porphyrins and Related Compounds*, Oxford University Press, Oxford, 1997.
2 K. M. Smith, *Porphyrins and metalloporphyrins: A New Edition Based on the Original Volume*, ed. J. E. Falk, Elsevier Sci Pub Co, New York, 1975.
3 S. Shanmugathasan, C. Edwards and R. W. Boyle, *Tetrahedron*, 2000, **56**, 1025–1046.
4 K. M. Kadish, K. M. Smith and R. Guilard. *The porphyrin handbook vol. 6, Applications: Past, Present and Future*, Academic Press, San Diego, 2000.
5 V. S. Da Silva, S. Nakagaki, G. M. Ucoski, Y. M. Idemori and G. DeFreitas-Silva, *RSC Adv.*, 2015, **5**, 106589–106598.
6 B. Meunier, *Chem. Rev.*, 1992, **92**, 1411–1456.
7 D. Dolphin, T. G. Traylor and L. Y. Xie, *Acc. Chem. Res.*, 1997, **30**, 251–259.
8 J. I. T. Costa, A. T. Tomé, M. G. P. M. S. Neves and J. A. S. Cavaleiro, *J. Porphyrins Phthalocyanines*, 2011, **15**, 1116–1133.
9 P. Battioni, O. Brigaud, H. Desvaux, D. Mansuy and T. G. Traylor, *Tetrahedron Lett.*, 1991, **32**, 2893–2896.
10 F. B. Zanardi, I. A. Barbosa, P. C. S. Filho, L. D. Zanatta, D. L. Silva, A. O. Serra and Y. Iamamoto, *Microporous Mesoporous Mater.*, 2016, **219**, 161–171.
11 K. A. D. F. Castro, F. H. C. Lima, M. M. Q. Simões, M. G. P. M. S. Neves, F. A. A. Paz, R. F. Mendes, S. Nakagaki and J. A. S. Cavaleiro, *Inorg. Chim. Acta*, 2017, **455**, 575–583.
12 N. B. McKeown, S. Hanif, K. Msayib, C. E. Tattershall and P. M. Budd, *Chem. Commun.*, 2002, 2782–2783.
13 A. R. Antonangelo, C. Grazia Bezzu, S. S. Mughal, T. Malewschik, N. B. McKeown and S. Nakagaki, *Catal. Commun.*, 2017, **99**, 100–104.
14 N. B. McKeown, *ISRN Mater. Sci.*, 2012, 1–16.
15 N. U. Day, C. C. Wamser and M. G. Walter, *Polym. Int.*, 2015, **64**, 833–857.
16 Y. Matsuo, J. Hatano and T. Nakagawa, *J. Phys. Org. Chem.*, 2014, **27**, 87–93.
17 H. L. Anderson, *Chem. Commun.*, 1999, 2323–2330.
18 H. Saltzmann and J. G. Sharefkin, *Org. Synth.*, 1963, **43**, 60–61.
19 J. S. Lindsey, I. C. Schreiman, H. C. Hsu, P. C. Kearney and A. M. Marguerettaz, *J. Org. Chem.*, 1987, **52**, 827–836.
20 C.-H. Lee and J. S. Lindsey, *Tetrahedron*, 1994, **50**, 11427–11440.
21 K. Singh, S. Behal and M. S. Hundal, *Tetrahedron*, 2005, **61**, 6614–6622.
22 B. J. Littler, Y. Ciringh and J. S. Lindsey, *J. Org. Chem.*, 1999, **64**, 2864–2872.

23 A. D. Adler, F. R. Longo, F. Kampas and J. Kim, *J. Inorg. Nucl. Chem.*, 1970, **32**, 2443–2445.
24 G. M. Sheldrick, *Acta Crystallogr., Sect. C: Cryst. Struct. Commun.*, 2015, **71**, 3–8.
25 O. V. Dolomanov, L. J. Bourhis, R. J. Gildea, J. A. K. Howard and H. Puschmann, *J. Appl. Crystallogr.*, 2009, **42**, 339–341.
26 G. R. Geier, B. J. Littler and J. S. Lindsey, *J. Chem. Soc., Perkin Trans. 2*, 2001, 701–711.
27 F. R. Kooriyaden, S. Sujatha, B. Varghese and C. Arunkumar, *J. Fluorine Chem.*, 2015, **170**, 10–16.
28 K. Tashiro, K. Konishi and T. Aida, *J. Am. Chem. Soc.*, 2000, **122**, 7921–7926.
29 G. G. Meng, B. R. James and K. A. Skov, *Can. J. Chem.*, 1994, **72**, 1894–1909.
30 M. Gouterman, *J. Mol. Spectrosc.*, 1961, **6**, 138–163.
31 J. Dalton, L. R. Milgrom and S. M. Pemberton, *J. Chem. Soc., Perkin Trans. 2*, 1980, 370–372.
32 C. J. P. Monteiro, M. M. Pereira, M. G. H. Vicente and L. G. Arnaut, *Tetrahedron*, 2012, **68**, 8783–8788.
33 V. N. Nemykin and R. G. Hadt, *J. Phys. Chem. A*, 2010, **114**, 12062–12066.
34 C. Chen and S. J. Hsieh, *J. Chin. Chem. Soc.*, 1997, **44**, 23–31.
35 J. R. Weinkauf, S. W. Cooper, A. Schweiger and C. C. Wamser, *J. Phys. Chem. A*, 2003, **107**, 3486–3496.
36 T. P. Wijesekera and D. Dolphin, *Synthetic aspects of porphyrin and metalloporphyrin chemistry*, R. A. Sheldon, New York, 1994, ch. 7.
37 L. J. Boucher, *J. Am. Chem. Soc.*, 1970, **92**, 2725–2730.
38 M. T. Caudle, C. K. Mobley, L. M. Bafaro, R. LoBrutto, G. T. Yee and T. L. Groy, *Inorg. Chem.*, 2004, **43**, 506–514.
39 L. J. Farrugia, *J. Appl. Crystallogr.*, 2012, **45**, 849–854.
40 A. L. Spek, *Acta Crystallogr., Sect. D: Biol. Crystallogr.*, 2009, **65**, 148–155.
41 C. Paliteiro and A. Sobral, *Electrochim. Acta*, 2005, **50**, 2445–2451.
42 J. Y. Inisan, R. Saillard, A. Guilard, Y. Tabard and L. Mest, *New J. Chem.*, 1998, **22**, 823–830.
43 K. M. Kadish, Z. Ou, R. Zhan, T. Khoury, E. Wenbo and M. J. Crossley, *J. Porphyrins Phthalocyanines*, 2010, **14**, 866–876.
44 L. J. Boucher and H. K. Garber, *Inorg. Chem.*, 1970, **9**, 2644–2649.
45 R. D. Arasasingham and T. C. Bruice, *Inorg. Chem.*, 1990, **29**, 1422–1427.
46 G. Ukoski, S. Nakagaki and F. S. Nunes, *J. Porphyrins Phthalocyanines*, 2014, **18**, 1–8.
47 G. R. Friedermann, M. Halma, K. A. D. F. Castro, F. L. Benedito, F. G. Doro, S. M. Drechsel, A. S. Mangrich, M. D. Assis and S. Nakagaki, *Appl. Catal., A*, 2006, **308**, 172–181.
48 K. A. D. F. Castro, M. M. Q. Simões, M. G. P. M. S. Neves, J. A. S. Cavaleiro, F. Wypych and S. Nakagaki, *Catal. Sci. Technol.*, 2014, **4**, 129–141.
49 K. A. D. F. Castro, M. M. Q. Simões, M. G. P. M. S. Neves, J. A. S. Cavaleiro, R. R. Ribeiro, F. Wypych and S. Nakagaki, *Appl. Catal., A*, 2015, **503**, 9–19.
50 G. K. B. Ferreira, K. A. D. F. Castro, G. S. Machado, R. R. Ribeiro, K. J. Ciuffi, G. P. Ricci, J. A. Marques and S. Nakagaki, *J. Mol. Catal. A: Chem.*, 2013, **378**, 263–272.
51 J. T. Groves, R. C. Haushalter, M. Nakamura, T. E. Nemo and B. J. Evans, *J. Am. Chem. Soc.*, 1981, **103**, 2884–2886.
52 W. Nam, I. Kim, M. H. Lim, H. J. Choi, J. S. Lee and G. H. Jang, *Chem.–Eur. J.*, 2002, **8**, 2067–2071.
53 J. T. Groves, W. T. Kruper and R. C. Haushalter, *J. Am. Chem. Soc.*, 1980, **102**, 6315–6371.